Transient climate response in a two-box energy-balance model. Part II: representation of the efficacy of deep-ocean heat uptake and validation for CMIP5 AOGCMs.

O. Geoffroy *, D. Saint-Martin, G. Bellon and A. Voldoire

Centre National de Recherches Météorologiques (CNRM-GAME), Toulouse, France

D. J. L. Olivié

Center for International Climate and Environmental Research - Oslo (CICERO), Oslo, Norway

and

University of Oslo, Oslo, Norway

S. Tytéca

Centre National de Recherches Météorologiques (CNRM-GAME), Toulouse, France

* *Corresponding author address:* Olivier Geoffroy, Centre National de Recherches Météorologiques (CNRM-GAME) 42 av. G. Coriolis, 31057 Toulouse, France.

E-mail: olivier.geoffroy@meteo.fr

ABSTRACT

In this second part of a series of two articles analyzing the global thermal properties of atmosphere-ocean coupled General Circulation Models (AOGCMs) within the framework of a two-box Energy Balance Model (EBM), the role of the efficacy of deep-ocean heat uptake is investigated. Taking into account such an efficacy factor is shown to amount to representing the effect of deep-ocean heat uptake on the local strength of the radiative feedback in the transient regime. It involves an additional term in the formulation of the radiative imbalance at Top-of-the-Atmosphere (TOA) that explains the nonlinearity between radiative imbalance and mean surface temperature observed in some AOGCMs. An analytical solution of this system is given and this simple linear EBM is calibrated for the set of 12 CMIP5 AOGCMs studied in Part I. It is shown that both net radiative fluxes at TOA and global surface temperature transient response are well represented by the simple EBM over the available period of simulations. Differences between this two-box EBM and the previous version without efficacy factor are analyzed and relationships between parameters are discussed. The simple model calibration applied to AOGCMs constitutes a new method for estimating their respective equilibrium climate sensitivity and adjusted radiative forcing amplitude from short-term step-forcing simulations and more generally a method to compute their global thermal properties.

1. Introduction

In Part I (Geoffroy et al. 2012, hereafter G12), it is shown using the CMIP5 database that a two-box energy-balance model calibrated only from an AOGCM step-forcing experiment is able to reproduce gradual CO_2-increase idealized scenarios. Such a calibration gives the first-order global thermal properties characterizing an AOGCM. The calibration method requires to determine both the reference radiative forcing amplitude and the equilibrium climate sensitivity (ECS), defined as the equilibrium mean surface temperature response for a $2xCO_2$ radiative perturbation.

Determining the amplitude of the radiative forcing associated with a given externally-imposed perturbation, and the ECS remain an issue and a topic of debate in the literature [e.g. Knutti and Hegerl (2008)]. While the evaluation of the radiative forcing is complicated by the existence of fast stratospheric and tropospheric adjustments (Gregory and Webb 2008), the determination of the ECS requires very long simulations (thousands of years) and is computationally expensive. Alternative methods have been proposed for estimating the equilibrium climate sensitivity. For example, it can be evaluated by coupling the atmospheric general circulation model (AGCM) to a mixed-layer ocean (ML). However, on the one hand, such an estimation remains computationally expensive. On the other hand, an AOGCM and its AGCM-ML counterparts estimates of the ECS may differ because the ocean circulation redistributes the energy and impacts the Earth's energy balance through its interaction with atmospheric processes.

Another type of methods consists in extrapolating the transient regime AOGCMs response to equilibrium. These methods lie on the linear assumption between the TOA radiative imbalance N and the mean surface temperature response: $N = \mathcal{F} - \lambda T$. Murphy (1995) introduced the effective climate sensitivity such that it can be deduced from the non-balanced mean surface temperature response and the amplitude of the radiative imbalance: $\mathrm{ECS}/T(t) = \mathcal{F}_{2\mathrm{xCO}_2}/(\mathcal{F}_{2\mathrm{xCO}_2} - N(t))$. But this estimation requires the knowledge of the radiative forcing $\mathcal{F}_{2\mathrm{xCO}_2}$ that must be deduced by an independent method. Gregory et al.

(2004) refined the estimate of the effective ECS by fitting the net radiative flux at TOA as a function of T along the whole period of an abrupt 2xCO_2 or a stabilization scenario. This introduces the concept of effective forcing. Such a fit gives the effective forcing (intercept), the effective radiative feedback parameter (slope) and the effective equilibrium climate sensitivity (x-axis intersection). The estimated forcing takes into account all the fast (few months) feedbacks that cannot be considered as feedbacks associated with the surface temperature response, such as stratospheric and tropospheric adjustments (Gregory and Webb 2008).

The main shortcoming of this type of methods is that the ECS is found to vary in time for some models and methods (Gregory et al. 2004; Senior and Mitchell 2000; Boer and Yu 2003b). This questions the validity of the linear assumption between N and T that is in the heart of energy-balance models (EBMs). Williams et al. (2008) showed that a bias in the estimation of the radiative forcing is partly responsible for these variations but not totally; the assumption of linearity itself has limitations. Indeed, one needs to distinguish between the temperature response induced by radiative flux for a given equilibrium temperature amplitude (i.e. a given radiative forcing) and for a given temperature amplitude in transient regime. Whereas the linear dependency assumption is reasonably robust in the first case, it is found not to be valid in the second case, at least for some climate models (Gregory et al. 2004; Williams et al. 2008; Winton et al. 2010).

Using CMIP3 idealized scenario simulations, Winton et al. (2010) showed that an additional process needs to be taken into account during the transient regime in order to represent the evolution of the radiative imbalance of the climate system. The ocean heat uptake reduces the rate of warming and this effect occurs preferentially in some regions, specially those corresponding to the sinking branches of the thermohaline circulation, in the North Atlantic ocean and circumpolar ocean of the southern hemisphere (Manabe et al. 1991). This modifies the transient regime temperature pattern in comparison with the equilibrium pattern. Because the feedback strength varies geographically, the pattern of surface temperature changes induced by the ocean heat uptake may impact the radiative imbalance in the transient regime. This reasoning led Winton et al. (2010) to introduce an efficacy factor for the ocean heat uptake. Held et al. (2010) introduced such an efficacy factor in the two-box linear EBM.

In this study, this simple model is used to determine the ECS, the adjusted radiative forcing and the thermal inertia properties of a given AOGCM by taking into account the effect of deep-ocean heat uptake on the radiative imbalance during the transient regime. This allows to compute all the parameters consistently in a single framework. In Section 2, the model with this feature is presented, underlying assumptions of the model are discussed and the calibration method is described. In Section 3, this method is applied to CMIP5 abrupt 4xCO_2 experiments. Results are discussed and compared to results obtained with the previous version of the EBM, without efficacy factor. The existence of relationships between the parameters is then investigated. Finally, a decomposition of the TOA net radiative flux in longwave and shortwave components is performed within the framework of this simple model.

2. Two-box model with an efficacy factor for deep-ocean heat uptake

a. System of equations and analytical solution

In this Part II, we consider the following two-box EBM with an efficacy factor for deep-ocean heat uptake ε proposed by Held et al. (2010):

$$C\frac{dT}{dt} = \mathcal{F} - \lambda T - \varepsilon\gamma(T - T_0), \tag{1}$$

$$C_0\frac{dT_0}{dt} = \gamma(T - T_0), \tag{2}$$

where C, C_0 and γ are respectively the first-layer (atmosphere/land/upper-ocean) surfacic heat capacity, the second-layer (deep-ocean) surfacic heat capacity and the heat exchange coefficient between the two layers. The term $\gamma(T - T_0)$ is the heat flux H exchanged between the two layers and is equal to the deep-ocean heat uptake: $H = \gamma(T - T_0)$. Since the change in the heat content of the first layer CdT/dt is driven by the sum of the heat flux exchanged with the deep ocean $-H$ and the heat flux exchanged with the external system N, the net radiative flux at TOA evolves as:

$$N = \mathcal{F} - \lambda T - (\varepsilon - 1)H. \tag{3}$$

In the following, EBM-1 will refer to the standard energy-balance model analyzed in G12 and EBM-ε to the model described above. The presence of an additional radiative flux term, $(\varepsilon - 1)H$, in the evolution of N constitutes the main difference with the EBM-1. In the case of a gradual increase of the external perturbation, CdT/dt is small (see G12); in the limit of negligible CdT/dt, $N = H$ and Eq. (3) leads to the formulation of Winton et al. (2010) [see their Eq. (3)]:

$$T_{eq} - T = \frac{\varepsilon}{\lambda} N, \tag{4}$$

with the equilibrium temperature response defined as $T_{eq} = \mathcal{F}/\lambda$.

By introducing $C_0' = \varepsilon C_0$ and $\gamma' = \varepsilon\gamma$, the system can be written as follows:

$$C\frac{dT}{dt} = \mathcal{F} - \lambda T - \gamma'(T - T_0), \tag{5}$$

$$C_0'\frac{dT_0}{dt} = \gamma'(T - T_0), \tag{6}$$

which is the same mathematical system as that of the EBM-1 except for the primes. As pointed by Held et al. (2010), the effect of the deep-ocean efficacy factor is equivalent to modifying ocean properties such that its surfacic heat capacity and the heat exchange coefficient between the two layers are scaled by a factor ε. Note that the EBM-ε is physically different from the EBM-1 because it includes an additional process. As a result, all the physical parameters estimated on the basis of this model can be different from their counterparts estimated within the framework of the EBM-1. The derivation of the analytical solution of the EBM-ε is straightforward. All the formulations of the eigenmode parameters given in G12 are still valid by replacing C_0 (respectively, γ) by C_0' (resp., γ'). These parameters are noted with the primes in the following. For a step forcing and a linear forcing with an increase rate F, the mean surface temperature response is, respectively:

$$T(t) = \frac{\mathcal{F}}{\lambda} - \frac{\mathcal{F}}{\lambda} a_f' e^{-t/\tau_f'} + \frac{\mathcal{F}}{\lambda} a_s' e^{-t/\tau_s'}, \tag{7}$$

$$T(t) = \frac{F}{\lambda} t - \frac{F}{\lambda} \tau_f' a_f' (1 - e^{-t/\tau_f'}) - \frac{F}{\lambda} \tau_s' a_s' (1 - e^{-t/\tau_s'}), \tag{8}$$

where τ_f', a_f', τ_s' and a_s' are the fast and slow eigenmode parameters defined in G12 and expressed as functions of λ, C, C_0' and γ'.

b. EBM-ε underlying hypothesis

1) Global budget

In this section, the hypothesis underlying the introduction of an efficacy factor ε are presented. Within the framework of a two-layer simple climate model, the change in the heat content of the climate system is the sum of the atmosphere/land/upper-ocean instantaneous heat uptake CdT/dt and the deep-ocean instantaneous heat uptake $C_0 dT_0/dt$. This change is equal to the net radiative imbalance N at the top of the atmosphere:

$$C\frac{dT}{dt} + C_0\frac{dT_0}{dt} = N. \tag{9}$$

Thus N can be decomposed into two radiative contributions N_U and N_D equal to the instantaneous rate of heat storage respectively in the upper and the deep oceans. Similarly, the temperature associated with the heat-uptake $T_H = T - T_{eq}$ (Winton et al. 2010; Geoffroy et al. 2012) can be decomposed into the sum of an upper-ocean contribution and a deep-ocean contribution: $T_H = T_U + T_D$. It is then assumed that the contributions to the TOA radiative imbalance induced by upper- and deep-ocean heat uptakes N_U and N_D are linear functions, respectively, of T_U with a feedback parameter λ and of T_D with a feedback parameter λ_D:

$$C\frac{dT}{dt} = N_U = -\lambda T_U, \tag{10}$$

$$C_0\frac{dT_0}{dt} = H = N_D = -\lambda_D T_D. \tag{11}$$

The deep-ocean heat-uptake temperature is associated with a different feedback parameter λ_D because the spatial pattern of the deep-ocean heat-uptake temperature differs from the equilibrium surface temperature response pattern. Following Hansen et al. (2005), Held et al. (2010) and Winton et al. (2010), an efficacy factor for deep-ocean heat uptake is introduced:

$$\varepsilon = \lambda/\lambda_D. \tag{12}$$

Summing Eqs. (10) and (11) leads to:

$$C\frac{dT}{dt} + H = -\lambda T_U - \frac{\lambda}{\varepsilon} T_D. \tag{13}$$

By using $T - T_{eq} = T_U + T_D$ and $H = -\lambda_D T_D$, Eq. (13) is equivalent to Eq. (1).

2) Local budget

To understand why the feedback strength may vary with the temperature pattern, it can be useful to examine the evolution of the local energy balance in transient regime. As pointed by Boer and Yu (2003a), the change in heat content of a climate system column is equal to the local radiative imbalance and the local convergence of the horizontal energy:

$$\frac{dh^i}{dt} + \frac{dh_0^i}{dt} = \mathcal{F}^i - \lambda^i T^i + A_t^i + A_{0t}^i, \tag{14}$$

where dh^i/dt and dh_0^i/dt are the local change in the heat content respectively of the first and the second layer; T^i, $\mathcal{F}^i$ and λ^i are respectively the local temperature response, the local forcing and the local feedback parameter; A_t^i and A_{0t}^i are the local convergence of the horizontal energy flux respectively of the first and the second layer. The superscript "i" denotes local values. The average over the Earth's surface of dh^i/dt (respectively, dh_0^i/dt)

is the change in the heat content of the first layer CdT/dt (respectively, of the second layer $C_0 dT_0/dt = H$). The global mean of the local forcing is $\mathcal{F}$. The global average of each local energy convergence A_t^i and A_{0t}^i is 0. Note that the local heat flux from the upper ocean to the deep ocean H^i verifies:

$$\frac{dh_0^i}{dt} = H^i + A_{0t}^i. \tag{15}$$

Equation (14) can be viewed as the heat budget in response to the sum of three "forcings": the external forcing $\mathcal{F}^i$ and two sink terms, the upper-ocean heat uptake dh^i/dt and the deep-ocean heat uptake dh_0^i/dt, being considered as "internal forcings". By assuming additivity of the temperature response patterns (Forster et al. 2000; Boer and Yu 2003a), the local surface temperature response can be expressed as the sum of the balance response to these "forcings": $T^i = T_{eq}^i + T_U^i + T_D^i$, and the local budget (14) can be decomposed in the following system of equations:

$$\mathcal{F}^i - \lambda^i T_{eq}^i + A_{eq}^i + A_{0eq}^i = 0, \tag{16}$$

$$-\frac{dh^i}{dt} - \lambda^i T_U^i + A_U^i + A_{0U}^i = 0, \tag{17}$$

$$-\frac{dh_0^i}{dt} - \lambda^i T_D^i + A_D^i + A_{0D}^i = 0, \tag{18}$$

where T_U^i and T_D^i are the local upper-ocean and deep-ocean heat-uptake temperatures, i.e., the temperature responses to the upper-ocean and deep-ocean heat-uptake "forcings". A_{eq}^i, A_U^i and A_D^i, are the associated convergences of horizontal energy fluxes in the first layer, with $A_t^i = A_{eq}^i + A_U^i + A_D^i$. Similarly, A_{0eq}^i, A_{0U}^i and A_{0D}^i are the convergences of horizontal energy fluxes in the second layer. Note that the global average of each energy-flux convergence A_x^i and A_{0x}^i is zero. Assuming that A_{0U}^i is 0 leads to $A_{0D}^i = A_{0t}^i - A_{0eq}^i$. Also, the decomposition of T and A_t in sums, Eq. (14) and Eqs. (16)-(18) leave one degree of freedom in the definition of T_U^i, T_D^i, A_U^i and A_D^i.

Introducing the normalized equilibrium temperature amplitude function $r_{eq}^i = T_{eq}^i/T_{eq}$, the local heat budget at equilibrium is:

$$\mathcal{F}^i - \lambda^i r_{eq}^i T_{eq} + A_{eq}^i + A_{0eq}^i = 0. \tag{19}$$

One can note that the equilibrium temperature pattern, i.e. r^i_{eq}, depends on the local forcing, the local feedback and the amplitude of the local energy convergence. Thus, the total feedback parameter λ is the average of the local feedback parameter weighted by the equilibrium temperature pattern:

$$\lambda = \frac{1}{S}\iint r^i_{eq}\lambda^i dS. \tag{20}$$

This parameter will be referred as the equilibrium feedback parameter in the following.

By assuming the separability of time and space variables for T^i_U and T^i_D, they can be decomposed in the product of a time-varying global average T_x by a spatial pattern r^i_x. On one hand, the upper-ocean heat content change has a relaxation time that is lower than the typical scale of interannual variability. We expect the pattern of T^i_U to be similar to the equilibrium pattern. By defining A^i_U such that $-dh^i/dt + A^i_U$ is the projection of $-dh^i/dt + A^i_t - A^i_{eq}$ onto the pattern $\lambda^i r^i_{eq}$, we can impose that the pattern of T^i_U is the same as that of the equilibrium temperature: $r^i_U = r^i_{eq}$. Note that this equality is imposed by the initial conditions in the case of a step forcing: $T_U(0) = -T_{eq}(0)$ and $T^i_U(0) = -T^i_{eq}(0)$. On the other hand, the pattern of T_D depends on the local deep-ocean heat uptake and on the residual energy convergences. Because the pattern of the deep-ocean heat uptake is different from the pattern of the radiative forcing, T^i_D is assumed to be associated with a pattern $r^i_D \neq r^i_{eq}$. Averaging Eq. (18) over the Earth's surface leads to Eq. (11) with the following formulation of λ_D:

$$\lambda_D = \frac{1}{S}\iint r^i_D\lambda^i dS. \tag{21}$$

The weight coefficient r^i_D is different from the one in the equilibrium feedback parameter expression. If the strength of the local feedback λ^i is low in regions where the ocean heat-uptake induces a small temperature increasing rate (resulting in high values of r^i_D), then λ_D is lower than λ. Consequently, for a given amplitude of T_U and T_D, N_D is smaller, i.e., the climate system accumulates less heat.

To conclude Section 2b, the introduction of an efficacy factor for the deep-ocean heat uptake is the result of a decomposition of the temperature pattern as the sum of the temperature response patterns to the radiative forcing, the upper-ocean and the deep-ocean heat uptakes assuming a linear relationship between these "forcings" and their associated temperature responses. Because the spatial pattern of the temperature response to the deep-ocean heat uptake differs from the equilibrium pattern, the spatial heterogeneity of the radiative feedbacks strength involves that the magnitude of the global radiative feedback varies in time during a climate transition.

c. *Effect of efficacy factor of deep-ocean heat uptake*

In case of a step forcing, the analytical solutions for the upper-ocean and deep-ocean heat-uptake temperatures are:

$$T_U(t) = -\frac{\mathcal{F}}{\lambda}\left[f'_U a'_f e^{-t/\tau'_f} + s'_U a'_s e^{-t/\tau'_s}\right], \tag{22}$$

$$T_D(t) = -\frac{\mathcal{F}}{\lambda}\left[f'_D a'_f e^{-t/\tau'_f} + s'_D a'_s e^{-t/\tau'_s}\right]. \tag{23}$$

The expression, the order of magnitude and the sign of the fractional contributions a'_f, a'_s, f'_U, f'_D, s'_U and s'_D are given in G12 (by replacing C_0 and γ by, respectively, C'_0 and γ' in the expressions).

The theoretical temporal evolutions of T, T_U and T_D in the case of a step-forcing are represented in the upper panels of Fig. 1 for three values of efficacy factor: $\varepsilon < 1$, $\varepsilon = 1$ and $\varepsilon > 1$ and other parameters unchanged. The upper-ocean heat-uptake temperature T_U increases with the characteristic timescale τ'_f, and after few years, it tends to zero since the contribution s'_U of the slow mode to T_U is negligible: the upper-ocean reservoir is saturated. Concerning the deep-ocean heat-uptake temperature, the contributions of the slow and fast modes (s'_D and f'_D) are comparable but of opposite signs. The fast mode is predominant in the first few years and induces a decrease in T_D, i.e., the heat flux exchanged between the two layers H increases because T increases faster than T_0. After this first phase (with a characteristic duration of τ'_f), the slow mode becomes dominant and T_D increases slowly back to zero: the deep ocean accumulates less and less heat.

The middle panels of Fig. 1 represent the theoretical relationship between the radiative imbalance N and the mean surface temperature perturbation T during the transient regime, for the same values of ε. The intercept and the x-axis intersection are independent from the value of ε. Per definition, the intercept at $T = 0$ is the amplitude of the forcing $\mathcal{F}$ (Gregory et al. 2004). Similarly, the x-axis intersection is the equilibrium temperature response (the equilibrium climate sensitivity in the case of a 2xCO_2 perturbation per definition). Only the path to join these two points is altered when ε is modified.

With $\varepsilon = 1$, the net radiative flux varies linearly with the temperature. For $\varepsilon \neq 1$, the plots suggest that there are two distinct stages in the (N, T) response to an abrupt forcing. To understand this behaviour, it is convenient to decompose the net flux into the sum of its two components contribution N_U and N_D. In Fig. 1 (middle row), the evolutions of (N_U, T) and (N_D, T) are plotted respectively with gray solid lines and dash-dotted lines.

During the first period, corresponding to the fast mode response timescale, the two components (upper and deep oceans) contribute with a similar amplitude but with opposite trends to the temperature response and N varies roughly linearly with T. Indeed, neglecting the slow response term during this period, the time evolutions of N_U and N_D are proportional to that of T_H (and T); the scale factors are, respectively, $-\lambda f'_U$ and $-\lambda_D f'_D$, with $f'_U > 0$ and $f'_D < 0$. Accordingly, the radiative imbalance N as the sum of these two contributions evolves roughly linearly with T.

During the second period, the contribution of the upper ocean is negligible ($s'_U \ll 1$) and the net radiative flux is simply the contribution of the deep-ocean heat-uptake temperature: $-\lambda_D T_D$. Then, since $T_D \approx T - T_{eq}$, the radiative flux varies also roughly linearly with T. The sharp change in the trend of the (N, T) line corresponds to a time similar to the fast relaxation time. This analysis suggests that linear fits of the two asymptots of the (N, T) curve performed separately as in Gregory et al. (2004) give a good approximation of the radiative forcing $\mathcal{F}$ (as the intercept of the first fit), the equilibrium temperature T_{eq} (as the x-axis intersection of the second fit), and $\lambda_D = \lambda/\varepsilon$ (as the slope of the second fit).

The net radiative flux at the top of the atmosphere can also be decomposed as the sum of prognostic variables and physical parameters of the EBM-ε as shown in Eq. (3). The radiative imbalance N is the sum of a linear term $\mathcal{F} - \lambda T$ and a fraction $1 - \varepsilon$ of the instantaneous rate of heat storage in the deep ocean H. Their evolution in the (N, T) space is illustrated in Fig. 1 (third row). The linear term takes into account the fact that the surface temperature is not in equilibrium, which induces a radiative imbalance. The second term is a deviation from this linear radiative flux due to the non linear evolution of the temperature pattern. The magnitude of H reflects the magnitude of this deviation.

Initially, $H = 0, T = 0$ and the radiative imbalance is equal to the forcing. In equilibrium, as H is zero, the assumption of linear dependence between the radiative imbalance and the surface temperature remains valid. But during the transient regime, the net radiative flux is affected by the deep-ocean heat uptake. The parameter usually referred to as the effective feedback parameter $\lambda_{eff} = (\mathcal{F} - N)/T$ varies in time (if $\varepsilon \neq 1$) and needs to be distinguished from the equilibrium feedback parameter λ. Instead of λ_{eff}, a transient radiative feedback function λ_t should be considered, with:

$$\lambda_t = \lambda + (\varepsilon - 1)\gamma \frac{T - T_0}{T}. \tag{24}$$

The efficacy factor can be determined from gradual perturbation AOGCMs simulations (by neglecting Cdt/dt) but requires prior knowledge of the equilibrium climate sensitivity and feedback parameter (Winton et al. 2010). On the other hand, all the EBM-ε radiative and thermal inertia parameters can be consistently computed from a step-forcing AOGCM experiment (and a control simulation) only, by taking into account the time evolution of the transient radiative feedback function. In the next section, the method used to adjust the EBM-ε physical parameters to a given AOGCM is briefly described.

d. *Method for EBM-ε parameter calibration*

In comparison with the EBM-1, the EBM-ε has an additional radiative parameter ε that needs to be tuned consistently with the reference radiative forcing amplitude (e.g. $\mathcal{F}_{2xCO_2}$ for a 2xCO_2 perturbation) and the equilibrium feedback parameter λ from the N-T evolution. The physical parameters of the EBM-ε are computed iteratively using a step-forcing experiment. The parameters are initially set to the EBM-1 values ($\varepsilon = 1$, and parameters computed in G12). For each iteration i, the deep-ocean heat uptake $H^{(i-1)}$ is first evaluated using the analytical solutions and the thermal parameters computed at iteration $(i-1)$. Then, using Eq. (3), a multi-linear regression of N (AOGCM values) against the AOGCM surface temperature response T and $H^{(i-1)}$ provides the values of $\mathcal{F}^{(i)}$, $\lambda^{(i)}$ and $\varepsilon^{(i)}$:

$$N = \mathcal{F}^{(i)} - \lambda^{(i)} T - (\varepsilon^{(i)} - 1) H^{(i-1)}. \tag{25}$$

Finally the thermal inertia parameters $C^{(i)}$, $C_0'^{(i)}$ and $\gamma'^{(i)}$ are tuned by performing two fits of the surface temperature response following the methodology used for the EBM-1 calibration (see details in Section 3 of G12). Few iterations are found to be sufficient to obtain convergence. This method for estimating the equilibrium climate sensitivity, radiative parameters and thermal inertia parameters from a short-term step-forcing simulation will be referred in the following as the EBM-ε method. In the next section, the EBM-ε method is applied to 12 CMIP5 AOGCMs using the abrupt 4xCO_2 experiment, and results are compared to the EBM-1 estimates (which, for the radiative properties, correspond to the estimates from Gregory et al. (2004)'s method).

3. Validation for CMIP5 AOGCMs

a. *Radiative parameters and TOA net flux, comparison with the EBM-1*

For the same twelve AOGCMs of the CMIP5 database analyzed in G12, the EBM-ε method is applied and radiative parameter values are reported in Table 1. The values of deep-ocean heat-uptake efficacy factor are mostly greater than 1 (see also Fig. 4a). Only two models (INM and CNRM) have values of ε smaller than unity. The heat-uptake efficacy factor ranges from 0.83 to 1.82 with a multimodel mean value of 1.29 and an intermodel standard deviation of 0.27. These results are in very good agreement with the estimates of Winton et al. (2010) for some CMIP2 and CMIP3 models analysis despite methodological differences. Winton et al. (2010) derived the ε from 1% y^{-1} CO_2 increase experiments using equilibrium climate sensitivity mainly derived from AGCMs coupled with a mixed-layer ocean model and using forcing estimates taken from Solomon et al. (2007). The latter were computed from different sources and they took into account either only the stratospheric adjustment or both stratospheric and tropospheric adjustments [through the method of Gregory et al. (2004)], depending on cases. In this study, the efficacy factor ε, the radiative forcing and the equilibrium climate sensitivity are derived jointly in the single framework of the EBM-ε.

Figures 2 and 3 compare for each model the N-T plot for AOGCM results, EBM-ε fit, and Gregory et al. (2004)'s linear regression. For models with an efficacy factor near 1 (CNRM, IPSL, MIROC), the assumption of linearity between N and T is valid and the results from EBM-ε are close to that of the linear model. For models with large ε (CSIRO, MOHC, NCC, MPIM), the results from EBM-ε largely improve the fit of radiative imbalance versus temperature response compared to a linear fit. In particular, the EBM-ε is able to reproduce the two-stage behaviour of these models in the parameter space (N, T).

Figures 4b-d compare the values of $\mathcal{F}_{4\mathrm{xCO}_2}$, λ and $T_{eq4\mathrm{xCO}_2}$ obtained within the framework of the EBM-ε and those derived with the method described in Gregory et al. (2004). The three AOGCMs with ε larger than 1.5 are indicated in full black markers. For these models, the radiative forcing amplitude and the equilibrium climate sensitivity are larger than in the standard linear model estimate. Indeed for CSIRO and MOHC, the equilibrium temperature response for a 4xCO_2 perturbation is up to 2 K warmer than the value derived from the linear assumption. The multimodel mean is 0.5 K warmer. The radiative forcing is 1 to 2 W m^{-2} larger for large ε models and the multimodel mean is 0.6 W m^{-2} larger. Most models have a forcing lower than 7.5 W m^{-2} except CCCMA, MPIM and MIROC. The two latter have a forcing of the order of 9 W m^{-2}, which suggests a strong effect of the tropospheric adjustment. The change in the ECS is mainly due to a change in the forcing, the radiative feedback parameters being less impacted. Moreover, contrary to the forcing and the equilibrium temperature, the sign of the λ difference between the EBM-1 and the EBM-ε estimates is independent of the sign of ε-1. For example, for MOHC and CSIRO, λ is respectively larger and lower with the EBM-ε method whereas both have an ε value greater than 1. The multimodel radiative forcing and radiative feedback parameter standard deviations are roughly unchanged whereas the equilibrium temperature one increases from 1.6 to 2.1 K. The improved match of the temperature response and radiative imbalance evolution between the AOGCMs and the simple EBM suggests that the values estimated from the EBM-ε method are more accurate. However, a complete assessment of the EBM-ε would require to extend AOGCM experiments until equilibrium, i.e., over a period of 1000 to 1500 years.

b. Thermal inertia parameters and temperature, comparison with the EBM-1

The thermal inertia physical parameters and the relaxation times are given in Table 2 and represented as a function of their EBM-1 counterparts in Figs. 4e-i. The fast relaxation time scale τ_f is not impacted by the inclusion of the efficacy of deep-ocean heat uptake whereas the slow relaxation timescale τ_s is. The change in τ_s is mainly due to change in the heat exchange coefficient γ rather than in the deep-ocean surfacic heat capacity C_0. Models with

$\varepsilon > 1$ have a lower γ than in the EBM-1 framework. The inclusion of the effect represented by the deviation term $(1-\varepsilon)H$ upon the temperature response amounts to modifying the deep-ocean heat uptake such that the heat exchange coefficient is $\varepsilon\gamma$. The lack of efficacy factor in the EBM-1 is compensated by a large γ when $\varepsilon > 1$.

The EBM-1 also underestimates the upper-ocean surfacic heat capacity C. The estimate of C depends on the forcing estimation since it is evaluated through an estimation of the temperature tendency at t=0 that is equal to $\mathcal{F}/C$. Consequently, an underestimation of $\mathcal{F}$ leads to an underestimation of C. These results suggest that the lack of radiative effect associated with deep-ocean heat uptake introduces a bias in the EBM-1 estimates of the thermal inertia parameters. The standard deviation of γ, C_0 and C is reduced with the EBM-ε, respectively from 0.13 to 0.11 W m^{-2} K^{-1}, 71 to 58 W y m^{-2} K^{-1} (but slightly increased from 26 to 29 W y m^{-2} K^{-1} if the INM is excluded) and 0.8 to 0.6 W y m^{-2} K^{-1}. This shows that introducing a new degree of freedom reduces slightly the inter-model spread.

Figure 5 shows the temperature response of the three AOGCMs with the largest ε estimates (CSIRO, NCC, and MOHC) for the abrupt 4xCO_2 and the 1% y^{-1} CO_2 experiments, as well as the EBM-1 and the EBM-ε analytical solutions using the parameters estimated by the corresponding method on the basis of the abrupt 4xCO_2 experiment. The temperature responses are identical for both EBMs in both the abrupt 4xCO_2 and the 1% y^{-1} CO_2 simulations over the first 150 years, and they match the AOGCM responses. But, for the step-forcing scenario, the EBM-ε response diverges from the EBM-1 response after about 300 years. Only the second phase of the temperature evolution, the one driven by the slow component of the system, is modified by the introduction of an efficacy factor. This is consistent with the fact that only the slow relaxation timescale varies between the EBM-1 and the EBM-ε methods. The EBM-1 calibrated with the abrupt simulation is accurate enough to represent the temperature evolution over the centennial scale. However, compared to the EBM-ε estimates, the EBM-1 parameters are biased as a result of a bias in radiative parameters estimated following the method of Gregory et al. (2004).

c. Parameters dependency

In this section, the question of potential relationships between the EBM-ε parameters is investigated. Table 3 shows the multimodel correlations between parameters of the EBM-ε, and also between these parameters and the equilibrium temperature response. For the set of 12 models, a correlation coefficient higher than 0.58 is significant at the 95% confidence level. As expected, the anticorrelation between T_{eq} and λ is high, with a correlation coefficient of -0.86. No correlation is found between $\mathcal{F}$ and λ suggesting that the effect of fast tropospheric adjustment is independent of the surface temperature feedback. Consistently, the equilibrium temperature is independent of the adjusted forcing magnitude.

Raper et al. (2002) suggested a negative correlation between their heat exchange coefficient κ of the one-box model (that is similar to the parameter γ) and the radiative feedback parameter λ but Gregory and Forster (2008) and Plattner et al. (2008)'s analysis of CMIP3 models did not find such a correlation. Including an interactive deep ocean changes the formulation of deep-ocean heat uptake and impacts the relationship between the heat exchange coefficient (κ or γ) and the radiative feedback parameter λ. Indeed, the EBM-ε estimates of λ and γ are positively correlated, with a correlation coefficient of 0.42 that is too small to be significant. The correlation between the corresponding EBM-1 estimates is even weaker (0.13). These results support Gregory and Forster (2008) and Plattner et al. (2008)'s conclusions.

All but two of the correlation coefficients between parameter estimates are found to be unsignificant. Note that if the INM, which is somewhat of an outlier (see G12) is excluded, the correlations between parameters are even weaker, and further from the significant level. The equilibrium temperature and ε are significantly correlated, with a correlation coefficient of 0.64. The reasons for this are unclear. It is possible that models with a higher climate sensitivity are also models with a higher regional radiative feedback in the region where the warming is slower (which corresponds to a larger ε). Local radiative feedbacks and horizontal heat transports would need to be investigated in order to answer this question.

The heat exchange coefficient γ and the surfacic heat capacity C are significantly correlated with a correlation coefficient of 0.62. Models with a higher upper-ocean heat capacity are also models that allow a larger heat flux between the upper ocean and the deep ocean for a smaller temperature difference between the two layers. More heat is accumulated in the upper ocean and also more heat is transported to the deep ocean for a given surface temperature. This might be an artefact of the oversimplified modeling of heat uptake in the two-box model, or it might result from energy constraints on the heat uptakes: for given heat uptakes, a large C yields a small temperature response T, which has to be compensated by a large γ in order to maintain upper-to-deep oceanic heat flux (that equals the deep-ocean heat uptake).

d. Decomposition in longwave and shortwave contributions

In this section, the net TOA radiative flux is decomposed in longwave (LW) and shortwave (SW) components, respectively N^{LW} and N^{SW}. We introduce LW and SW radiative feedback parameters associated to the deep-ocean heat-uptake temperature, respectively λ_D^{LW} and λ_D^{SW} and we assume the decomposition in an upper-ocean and a deep-ocean radiative contribution is valid for each component separately. These assumptions yield the following equations:

$$N^{LW} = \mathcal{F}^{LW} - \lambda^{LW} T - (\lambda^{LW} - \lambda_D^{LW}) \frac{\varepsilon}{\lambda} H, \tag{26}$$

$$N^{SW} = \mathcal{F}^{SW} - \lambda^{SW} T - (\lambda^{SW} - \lambda_D^{SW}) \frac{\varepsilon}{\lambda} H, \tag{27}$$

where $\mathcal{F}^{LW}$, $\mathcal{F}^{SW}$, λ^{LW} and λ^{SW} are, respectively, the LW and the SW components of the radiative forcing and of the radiative feedback parameter. Unlike in the case of the total feedback, we do not define a SW or LW efficacy factor ε_{SW} or ε_{LW}. Indeed, although the total feedback is necessary different from zero, it is possible that λ^{SW} (λ_D^{SW}) is zero whereas λ_D^{SW} (λ^{SW}) is not. In such a case, a shortwave efficacy factor ε_{SW} would have no sense.

Each LW and SW component is calculated by multi-linear regression of the corresponding net radiation flux as a function of temperature (both from the AOGCM abrupt 4xCO_2 experiment) and $\frac{\varepsilon}{\lambda}H$ (from the EBM-ε estimation). Values of the tuned LW and SW radiative parameters are reported in Table 4 and resulting fits for each model separately shown in Figs. 6 and 7. These figures reflect the large intermodel spread in both forcing and radiative feedback parameters LW and SW components.

AOGCMs that have a large SW forcing contribution can have a large LW contribution (MPIM) or a small LW contribution (IPSL). The 4xCO_2 LW forcing ranges from 3.4 to 7.4 W m^{-2} with an ensemble mean of 6.1 W m^{-2} and a standard deviation of 1.1 W m^{-2}. The 4xCO_2 SW forcing is mostly positive with a mean value of 1.3 W m^{-2} except for two models (CSIRO, INM). Its standard deviation is slightly larger than the one of the LW contribution. By comparison with estimates taking into account the stratospheric adjustment only, the forcing is found to be lower in the LW and larger in the SW. Indeed, Forster and Taylor (2006) found a forcing estimate of 3.45 W m^{-2} in the LW for a 2xCO_2 experiment (corresponding to 6.90 W m^{-2} for a 4xCO_2 experiment). The instantaneous SW forcing is of the order of -0.06 W m^{-2} (Myhre et al. 1998). These estimates confirm Gregory and Webb (2008) and suggest a non negligible effect of the fast change in the cloud component (among the other feedbacks) on the radiative forcing adjustment. However, the LW and SW forcings are larger than Gregory and Webb (2008)'s estimates (respectively 2.84 and 0.50 W m^{-2} for an ensemble of 2xCO_2 experiments) which is consistent with $\varepsilon > 1$ for most models. Thus, for the majority of AOGCMs, the EBM-ε estimation decreases the LW contribution of the tropospheric adjustment and increases the SW contribution in comparison with an estimation based on a linear fit.

The LW contribution to the feedback parameter λ^{LW} is positive (i.e. negative feedback) for all models because the radiative imbalance is restored by increased LW emission associated with the temperature increase. The SW contribution to the feedback parameter λ^{SW} is negative (i.e. positive feedback) for all models except GFDL which has a negligible λ^{SW}.

For most AOGCMs, λ^{SW} is above (in absolute value) the 0.2-0.4 W m^{-2} K^{-1} typical range of the albedo feedback, suggesting a positive feedback of clouds in the SW.

The deep-ocean heat-uptake feedback parameter λ_D^{LW} is generally of the same order of magnitude as λ^{LW} but λ_D^{SW} is smaller than λ^{SW}. This suggests that the value of $\varepsilon > 1$ obtained for the majority of the models is mainly due to the shortwave radiation, with low clouds as a good candidate to explain most of the difference between EBM-ε and EBM-1. Further analysis is necessary to understand which components of the climate system are responsible for the differences and quantify each contribution. But the results of such a simple SW-LW decomposition suggest that the EBM-ε framework can be used to decompose the radiative fluxes such as a cloud/clear-sky decomposition or more complex decompositions such as partial radiative fluxes.

4. Conclusion

In this study, the two-box energy-balance model with an efficacy factor of deep-ocean heat uptake is used as a tool to estimate the first-order global thermal properties of AOGCMs. These thermal properties include both radiative properties and thermal inertia properties. It is shown that the temperature response can be decomposed as the balanced response to three ”forcings”: the TOA radiative forcing, the upper-ocean heat uptake and the deep-ocean heat uptake. Assuming additivity of each temperature response patterns to these ”forcings” and assuming the separability of time and spatial variability of these temperature responses, the radiative feedback parameter associated with the deep-ocean heat uptake is shown to be different from the equilibrium feedback parameter, seeing that the local feedback parameter varies geographically. This results in the presence of an additional term in the radiative imbalance formulation depending on the deep-ocean heat uptake.

Within this EBM-ε framework, the concepts of effective forcing and effective climate sensitivity are unchanged but the concept of effective feedback parameter is modified. The effective forcing remains the physical parameter defined by Gregory et al. (2004), i.e., the value of the net radiative imbalance when the temperature tends to zero. It is sensitive to fast feedbacks due to changes in both stratospheric and tropospheric variables, such as clouds, temperature lapse rate, and water vapour amount, associated with the external radiative perturbation, but unassociated with the surface temperature response. However, the effective climate feedback parameter such as usually defined, i.e., the feedback parameter of the transient regime, needs to be distinguished from the equilibrium feedback parameter. The effective equilibrium feedback parameter is assumed to be constant for a given type of forcing agent, a given spatial distribution of the forcing amplitude but it is valid only for an equilibrium state. The transient feedback function involves an additional term that can depend on deep-ocean heat uptake and it can thus vary in time.

An iterative method of calibration is proposed and applied to twelve CMIP5 AOGCMs. The results show that the model reproduces with accuracy the evolution of the radiative imbalance as a function of the temperature response during a transient regime. The fits of the temperature evolution over the time of simulation (about 150 years) are the same as those obtained with the EBM-1. However, the physical parameters of the model are different. The improved match of the temperature response and radiative imbalance evolution between the AOGCMs and the EBM suggests that the values estimated from the EBM-ε method are more accurate. Moreover, the method is applied to the LW and the SW component of the radiative flux. Each evolution separately is well represented suggesting that the method can be applied to partial decomposition of the radiative imbalance.

The benefit of two-box EBMs such as the EBM-1 and EBM-ε is that they are the simplest EBMs that represent both the beginning of the simulation (determined by the forcing) and the end of the experiment (determined by the equilibrium climate sensitivity for a constant forcing). One-box EBMs are unable to represent both phases of the time evolution. The advantage of the EBM-ε on the EBM-1 is that the net TOA imbalance is better represented as a function of the global surface temperature response. The EBM-ε can be used to compute the radiative parameters and the effective climate sensitivity consistently from one single methodology and one single short AOGCM experiment, by taking into account the time variation of the effective feedback function. From this point of view, the calibration of the EBM-ε method constitutes a new, improved method to determine the climate sensitivity and the adjusted forcing of an AOGCM.

Such two-box EBM offers a complete first-order explanation of the behaviour of climate models under an externally imposed perturbation. The spread on the radiative and thermal-inertia global parameters within a generation of models (such as the CMIP5 generation) can be used as a indication of the uncertainty of the multi-model climate projections performed for the Intergovernmental Panel on Climate Change. The evolution of this spread from one CMIP exercise to the next indicates whether AOGCMs converge in terms of global properties. It can also be used for AOGCM's analysis, by relating some of the EBM parameters to physical processes or physical variables that can be directly calculated in the AOGCM. In parallel, the calibration of such model, that could be extended to other type of radiative perturbations, offers a physically-based simple climate model able to emulate the AOGCM response to different idealized scenarios.

Acknowledgments.

We thank Julien Boé, Aurélien Ribes and Laurent Terray for helpful discussions and valuable comments on the work. Thanks are also due to Isaac Held for sharing interesting ideas in his blog. This work was supported by the European Union FP7 Integrated Project COMBINE.

REFERENCES

Boer, G. and B. Yu, 2003a: Climate sensitivity and climate response. *Clim. Dyn.*, **20**, 415–429.

Boer, G. and B. Yu, 2003b: Climate sensitivity and climate state. *Clim. Dyn.*, **21**, 167–176.

Forster, P. M., M. Blackburn, R. Glover, and K. P. Shine, 2000: An examination of climate sensitivity for idealised climate change experiments in an intermediate general circulation model. *Clim. Dyn.*, **16**, 833–849.

Forster, P. M. and K. E. Taylor, 2006: Climate forcings and climate sensitivities diagnosed from coupled climate model integrations. *J. Climate*, **19**, 61816194.

Geoffroy, O., D. Saint-Martin, D. J. L. Olivié, A. Voldoire, G. Bellon, and S. Tytéca, 2012: Transient climate response in a two-box energy-balance model. Part I: analytical solution and parameter calibration using CMIP5 AOGCM experiments. *Submitted to J. Climate.*

Gregory, J. M. and M. Webb, 2008: Tropospheric adjustment induces a cloud component in CO_2 forcing. *J. Climate*, **21**, 58–71.

Gregory, J. M. and P. M. Forster, 2008: Transient climate response estimated from radiative forcing and observed temperature change. *J. Geophys. Res.*, **113**, D23 105.

Gregory, J. M., and Coauthors, 2004: A new method for diagnosing radiative forcing and climate sensitivity. *Geophys. Res. Lett.*, **31**, L03205, doi:10.1029/2003GL018747.

Hansen, J., and Coauthors, 2005: Efficacy of climate forcings. *J. Geophys. Res.*, **110**, D18104, doi:10.1029/2005JD005776.

Held, I. M., M. Winton, K. Takahashi, T. Delworth, F. Zeng, and G. K. Vallis, 2010: Probing the fast and slow components of global warming by returning abruptly to preindustrial forcing. *J. Climate*, **23**, 2418–2427.

Knutti, R. and G. C. Hegerl, 2008: The equilibrium sensitivity of the Earth's temperature to radiation changes. *Nature Geosc.*, **1**, 735–743.

Manabe, S., R. J. Stouffer, M. J. Spelman, and K. Bryan, 1991: Transient responses of a coupled-ocean atmosphere model to gradual changes of atmospheric CO2. Part I: Annual mean response. *J. Climate*, **4**, 785–818.

Murphy, J. M., 1995: Transient response of the Hadley Centre coupled Ocean-atmosphere model to increasing carbon dioxide. Part III: Analysis of global-mean response using simple models. *J. Climate*, **8**, 496–514.

Myhre, G., E. Highwood, K. Shine, and F. Stordal, 1998: New estimates of radiative forcing due to well mixed greenhouse gases. *Geophys. Res. Lett.*, **25**, 2715–2718.

Plattner, G.-K., and Coauthors, 2008: Long-term climate commitments projected with climate-carbon cycle models. *J. Climate*, **21**, 27212751.

Raper, S. C. B., J. M. Gregory, and R. J. Stouffer, 2002: The role of climate sensitivity and ocean heat uptake on AOGCM transient temperature response. *J. Climate*, **15**, 124–130.

Senior, C. A. and J. F. B. Mitchell, 2000: The time dependence of climate sensitivity. *Geophys. Res. Lett.*, **27**, 2685–2688.

Solomon, S., D. Qin, M. Manning, M. Marquis, K. B. Averyt, M. Tignor, H. L. Miller, and Z. Chen, 2007: *Climate Change 2007: The physical science basis.* Cambridge Univ. Press, New York.

Williams, K. D., W. J. Ingram, and J. M. Gregory, 2008: Time variation of effective climate sensitivity in GCMs. *J. Climate*, **21**, 5076–5090.

Winton, M., K. Takahashi, and I. M. Held, 2010: Importance of ocean heat uptake efficacy to transient climate change. *J. Climate*, **23**, 2333–2344.

List of Tables

TABLE 1. The $4xCO_2$ radiative forcing $\mathcal{F}_{4xCO_2}$, total feedback parameter λ, efficacy factor for deep-ocean heat uptake ε, and $4xCO_2$ equilibrium temperature T_{4xCO_2} estimates in the framework of the EBM-ε of the twelve CMIP5 models used in this paper, and their multimodel mean and standard deviation.

Model	$\mathcal{F}_{4xCO_2}$ (W m^{-2})	λ (W m^{-2} K^{-1})	ε	T_{4xCO_2} (K)
BCC (BCC-CSM1-1)	7.4	1.28	1.27	5.8
CCCMA (CanESM2)	8.2	1.06	1.28	7.8
CNRM (CNRM-CM5.1)	7.1	1.12	0.92	6.4
CSIRO (CSIRO-Mk3-6-0)	7.0	0.68	1.82	10.2
GFDL (GFDL-ESM2M)	7.1	1.38	1.21	5.1
INM (INMCM4)	6.0	1.56	0.83	3.9
IPSL (IPSL-CM5A-LR)	6.7	0.79	1.14	8.5
MIROC (MIROC5)	8.9	1.58	1.19	5.6
MOHC (HadGEM2-ES)	6.8	0.61	1.54	11.1
MPIM (MPI-ESM-LR)	9.4	1.21	1.42	7.8
MRI (MRI-CGCM3)	7.1	1.31	1.25	5.4
NCC (NorESM1-M)	7.4	1.15	1.57	6.5
Multimodel mean	7.4	1.14	1.29	7.0
Standard deviation	1.0	0.32	0.27	2.1

Table 2. The atmosphere/land/upper ocean surfacic heat capacity C, deep-ocean surfacic heat capacity C_0, heat exchange coefficient γ and fast and slow relaxation times estimates in the framework of the EBM-ε of the twelve CMIP5 models used in this paper, and their multimodel mean and standard deviation.

Model	C (W y m^{-2} K^{-1})	C_0 (W y m^{-2} K^{-1})	γ (W m^{-2} K^{-1})	τ_f (y)	τ_s (y)
BCC (BCC-CSM1-1)	8.4	56	0.59	4.1	152
CCCMA (CanESM2)	8.0	77	0.54	4.5	139
CNRM (CNRM-CM5.1)	8.3	95	0.51	5.2	266
CSIRO (CSIRO-Mk3-6-0)	8.5	76	0.71	4.2	316
GFDL (GFDL-ESM2M)	8.8	112	0.85	3.6	233
INM (INMCM4)	8.5	271	0.67	4.0	546
IPSL (IPSL-CM5A-LR)	8.1	100	0.57	5.5	327
MIROC (MIROC5)	8.7	158	0.73	3.6	338
MOHC (HadGEM2-ES)	7.5	98	0.49	5.4	457
MPIM (MPI-ESM-LR)	8.5	78	0.62	4.0	220
MRI (MRI-CGCM3)	9.3	68	0.59	4.4	181
NCC (NorESM1-M)	9.7	121	0.76	4.1	328
Multimodel mean	8.5	109	0.64	4.4	300
Standard deviation	0.6	58	0.11	0.7	113

TABLE 3. Intermodel correlations between the equilibrium temperature at $4xCO_2$ T_{4xCO_2} and the physical parameters $\mathcal{F}$, λ, ε, γ, C_0, C of the EBM-ε for the 12 CMIP5 AOGCMs.

	T_{4xCO_2}	$\mathcal{F}$	λ	ε	γ	C_0	C
T_{4xCO_2}	1	0.02	**-0.86**	**0.64**	-0.38	-0.45	-0.51
$\mathcal{F}$		1	0.23	0.18	0.06	-0.28	0.12
λ			1	-0.55	0.42	0.46	0.47
ε				1	0.14	-0.48	0.09
γ					1	0.29	**0.62**
C_0						1	0.06
C							1

TABLE 4. The LW and SW components of the radiative forcing, $\mathcal{F}^{LW}$ and $\mathcal{F}^{SW}$, of the total feedback parameter, λ^{LW} and λ^{SW}, and of the deep-ocean heat-uptake feedback parameter, λ_D^{LW} and λ_D^{SW}, estimates in the framework of the EBM-ε of the twelve CMIP5 models used in this paper, and their multimodel mean and standard deviation STDV.

Model	$\mathcal{F}^{LW}$ (W m^{-2})	$\mathcal{F}^{SW}$ (W m^{-2})	λ^{LW} (Wm^{-2}K^{-1})	λ^{SW} (Wm^{-2}K^{-1})	λ_D^{LW} (Wm^{-2}K^{-1})	λ_D^{SW} (Wm^{-2}K^{-1})
BCC	6.4	1.0	1.69	-0.42	1.68	-0.68
CCCMA	6.2	2.0	1.42	-0.37	1.38	-0.57
CNRM	5.1	2.1	1.62	-0.50	1.67	-0.46
CSIRO	7.4	-0.4	1.97	-1.29	1.81	-1.43
GFDL	5.4	1.7	1.37	0.01	1.68	-0.54
INM	6.8	-0.7	2.12	-0.55	2.65	-0.76
IPSL	3.4	3.3	1.92	-1.13	1.89	-1.20
MIROC	6.9	2.0	1.93	-0.35	1.70	-0.37
MOHC	6.2	0.6	1.56	-0.96	1.55	-1.16
MPIM	7.0	2.5	1.67	-0.46	1.50	-0.65
MRI	6.6	0.5	2.24	-0.93	2.16	-1.11
NCC	6.3	1.1	1.82	-0.67	1.67	-0.93
Mean	6.1	1.3	1.78	-0.63	1.78	-0.82
STDV	1.1	1.2	0.27	0.37	0.34	0.34

List of Figures

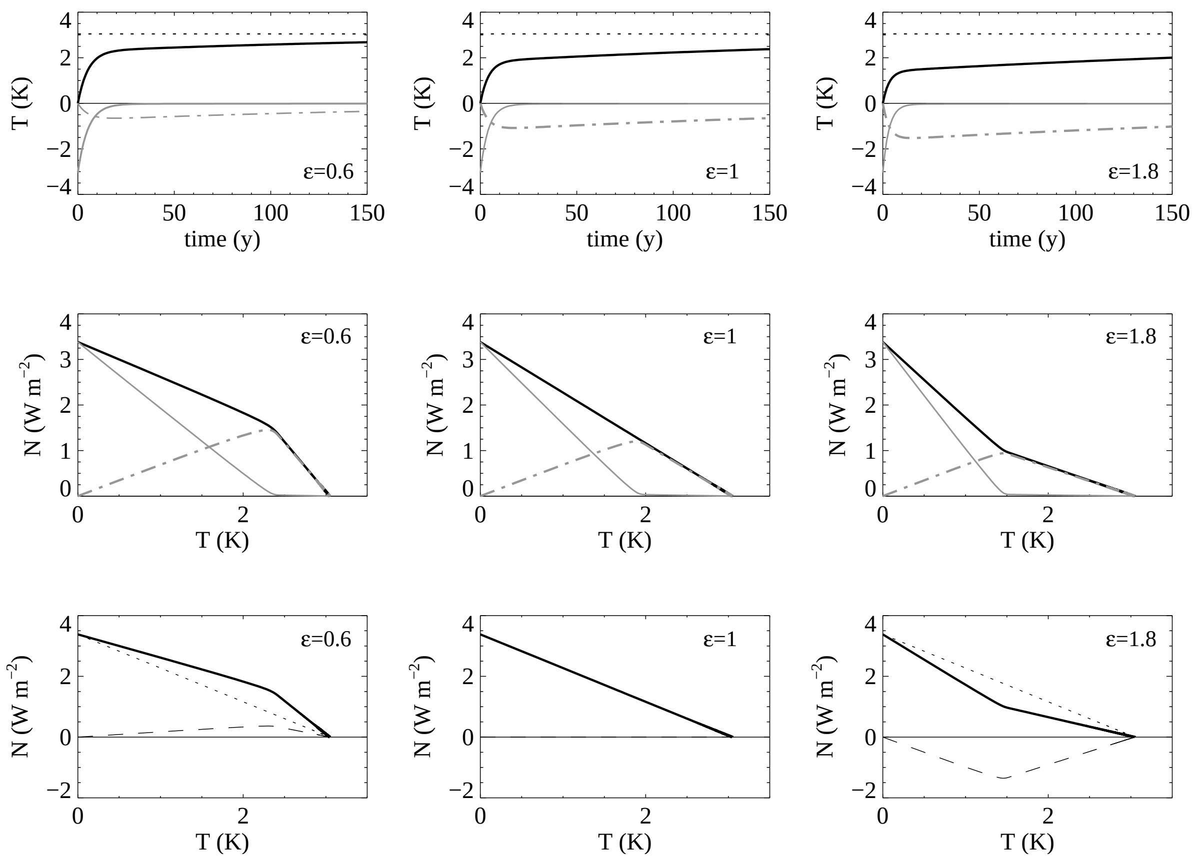

FIG. 1. EBM-ε results. Upper panels: time evolution of global mean surface air temperature (thick black), upper-ocean heat-uptake temperature T_U (thick grey) and deep-ocean heat-uptake temperature T_D (dot-dashed grey) for a step-forcing case; the black dotted line shows the equilibrium temperature T_{eq}. Middle panels: global mean net radiative flux (thick black) and its decomposition into $N_U = -\lambda T_U$ (thick grey) and $N_D = -\lambda_D T_D$ (dot-dashed grey) as functions of the global mean surface air temperature. Bottom panels: global mean net radiative flux (thick black, same as above) and its decomposition into the linear term $\mathcal{F} - \lambda T$ (dot grey) and the deviation term $-(\varepsilon - 1)H$ (dashed grey). Plots are for three ε values indicated on the panels and $\mathcal{F} = 3.9$ W m^{-2}, $\lambda = 1.3$ W m^{-2} K^{-1}, $C = 8$ W y m^{-2} K^{-1}, $C_0 = 100$ W y m^{-2} K^{-1}, $\gamma = 0.7$ W m^{-2} K^{-1}.

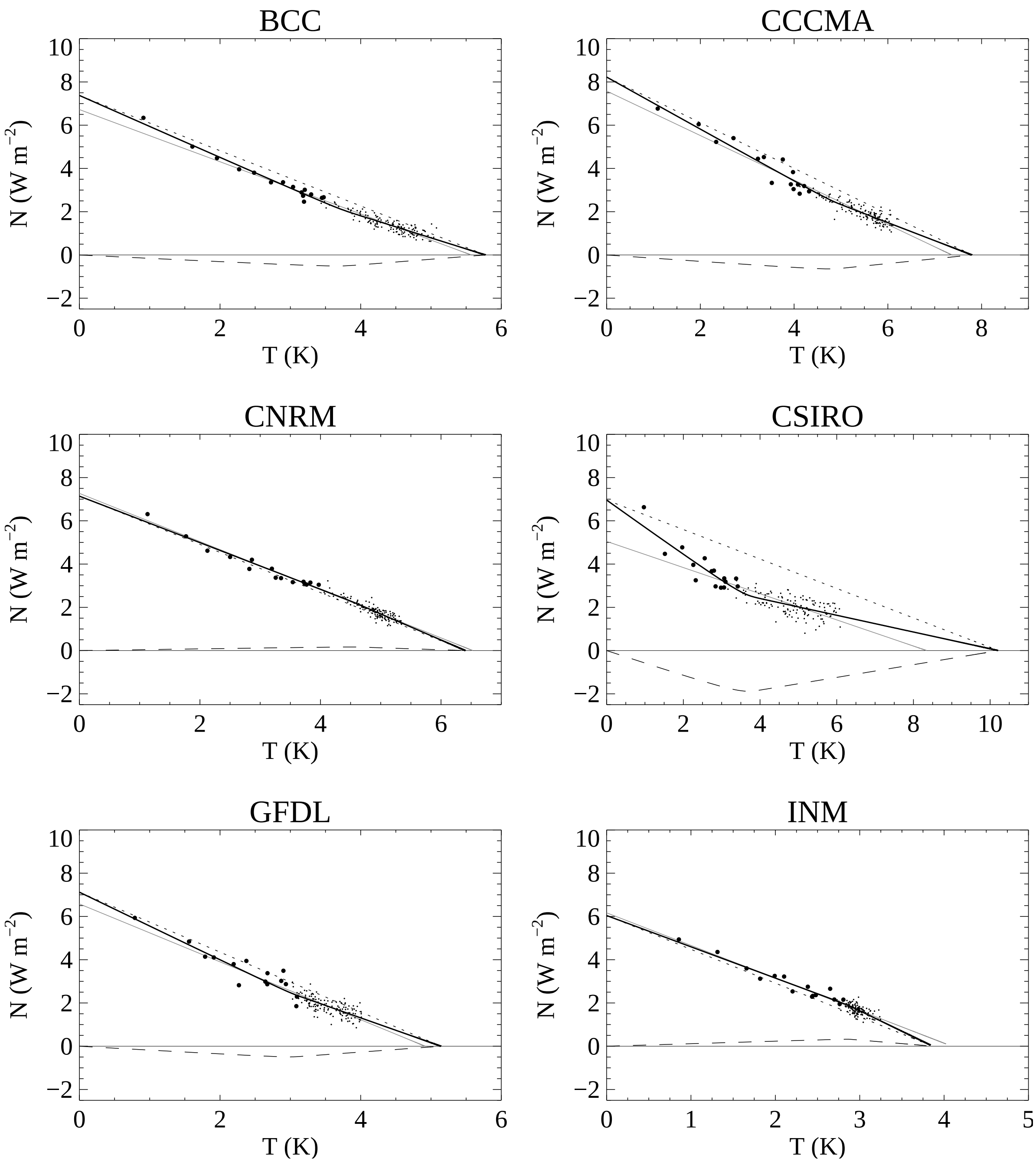

FIG. 2. Global mean net radiative flux at TOA N as a function of global mean surface air temperature T for the abrupt $4xCO_2$ experiments (black dots, large dots for the first 15 years), for 6 AOGCMs. The thick black line is the EBM-ε fit. The dotted and dashed lines show, respectively, the linear contribution $\mathcal{F} - \lambda T$ and the deviation contribution $-(\varepsilon - 1)H$. The grey line is Gregory et al. (2004)'s linear fit. The thin black line shows $N = 0$. Note that the range of T can differ from one panel to another.

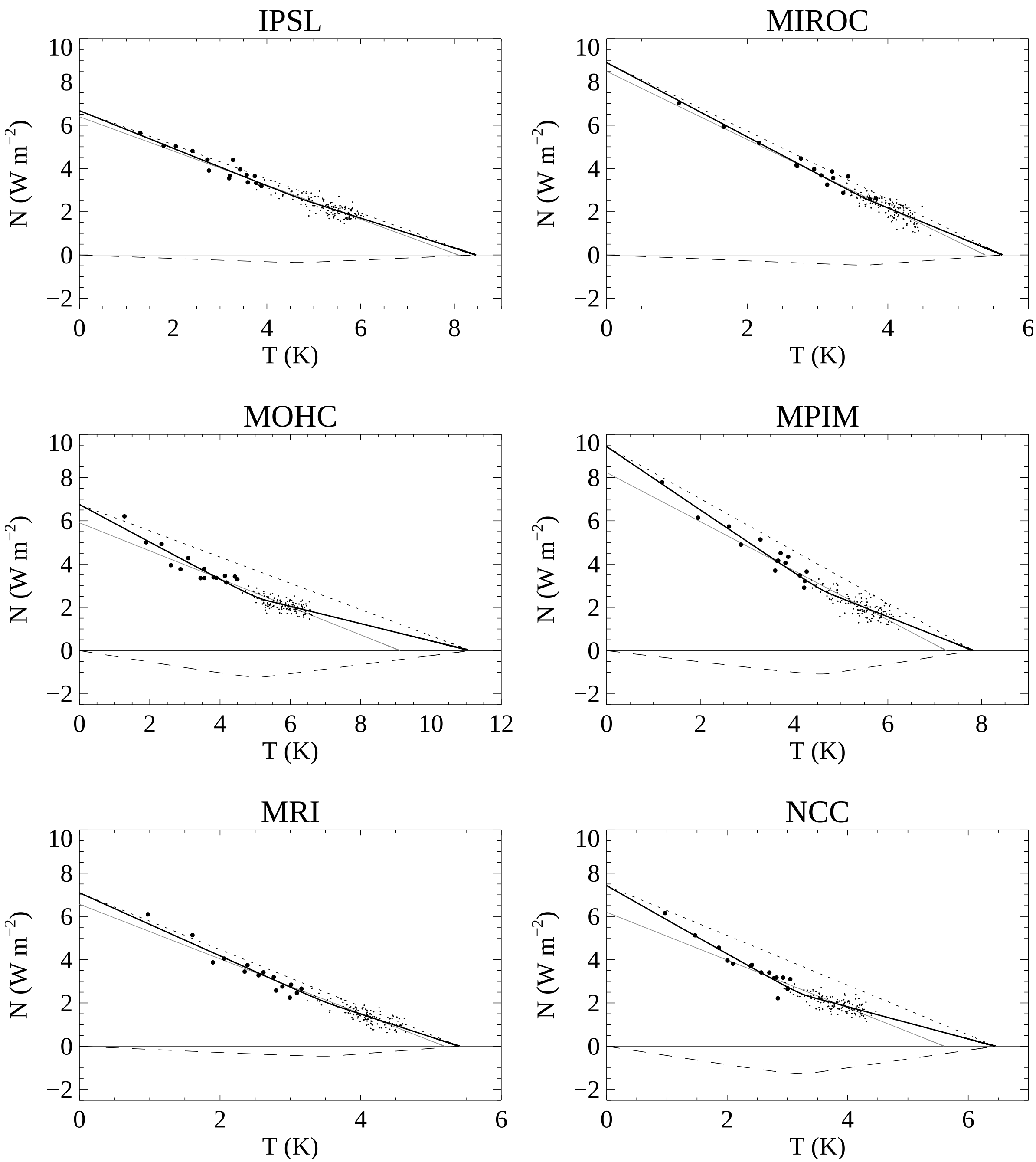

FIG. 3. Same as Fig. 2 for the 6 other AOGCMs.

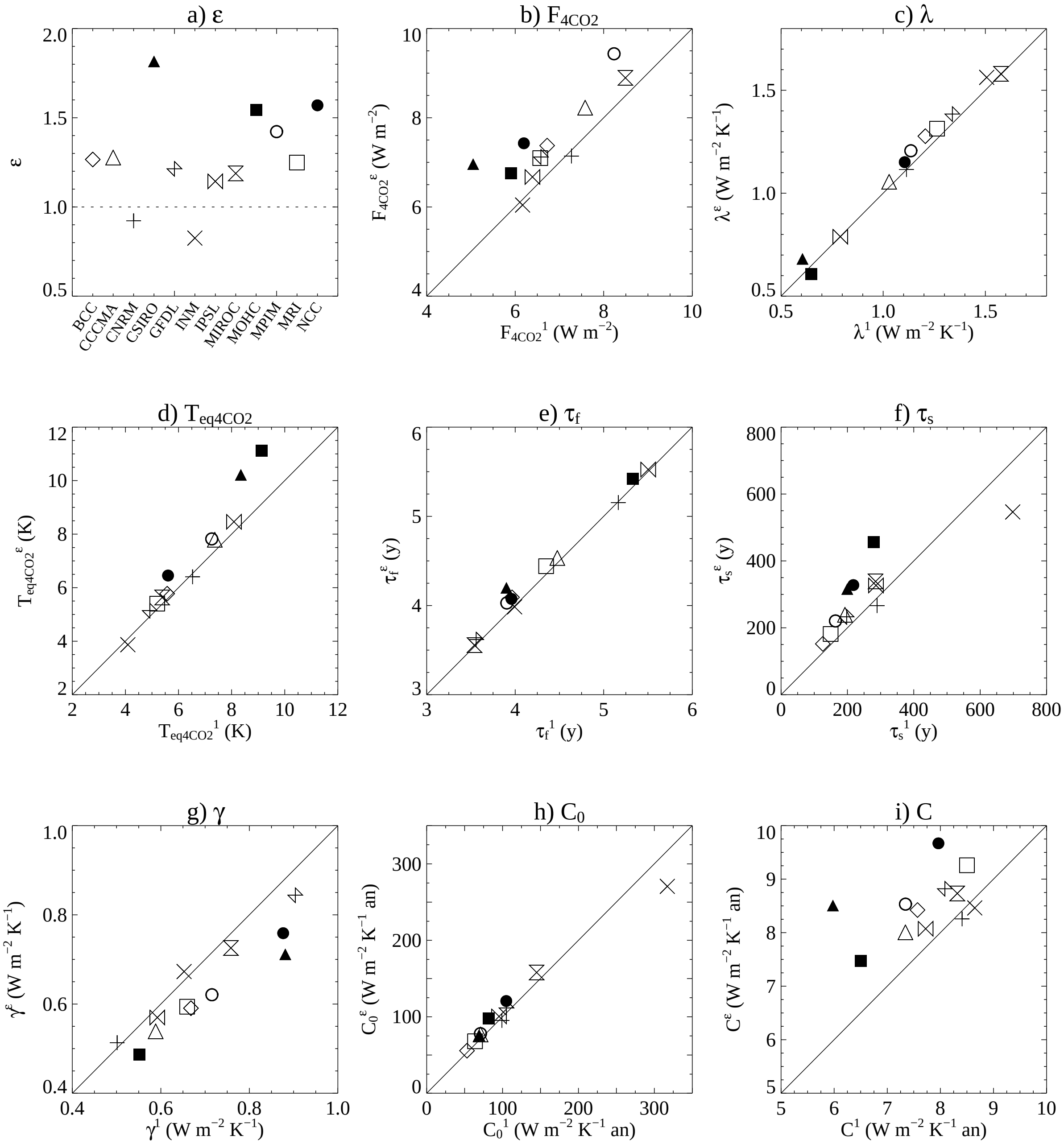

FIG. 4. Parameter estimates: ε values for the 12 AOGCMs (a) and EBM-ε estimates as a function of EBM-1 estimates for $\mathcal{F}_{4\mathrm{xCO_2}}$ (b), λ (c), $T_{eq4\mathrm{xCO_2}}$ (d), τ_f (e), τ_s (f), γ (g), C_0 (h), and C (i). Superscripts 1 and ε denote, respectively, estimates from the EBM-1 and the EBM-ε methods. The dotted line shows $\varepsilon = 1$ in (a), and the solid lines in (b)-(i) indicate a perfect match between EBM-ε and EBM-1 estimates.

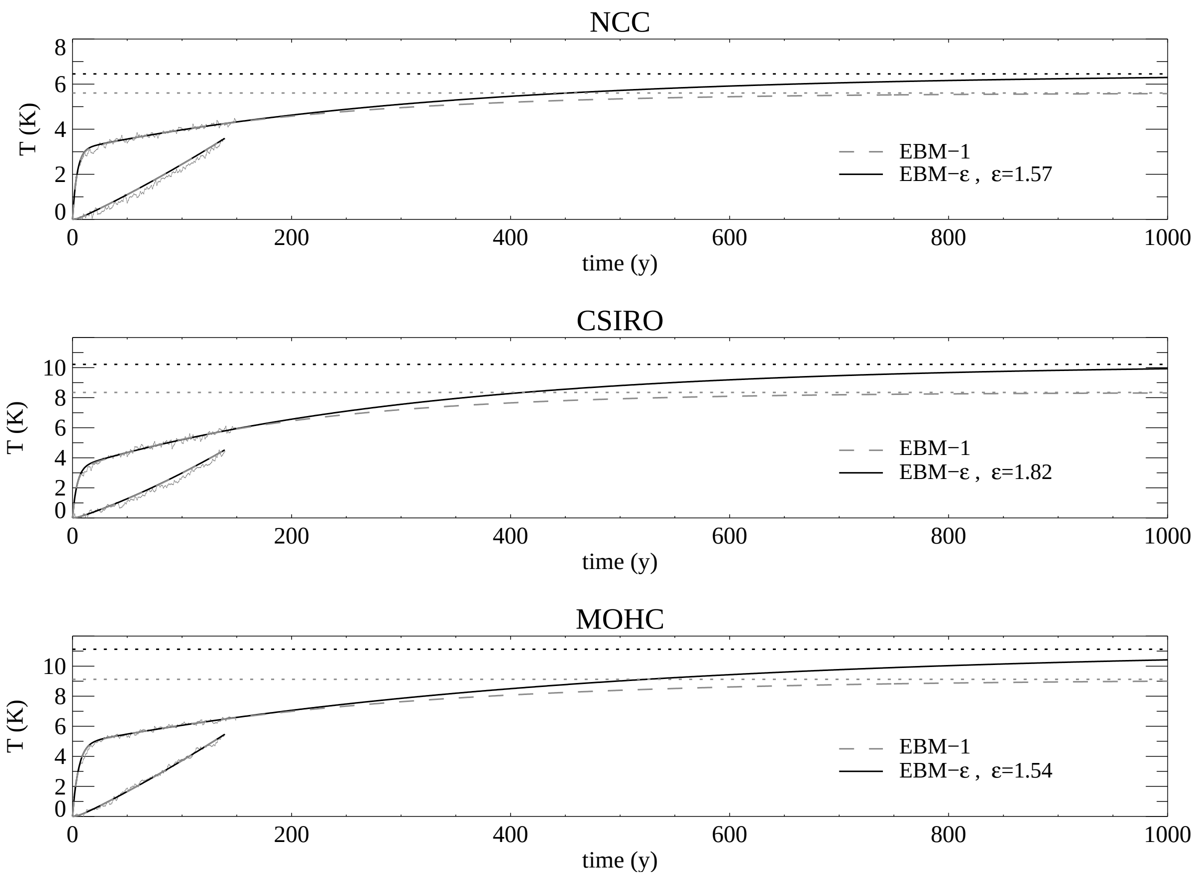

FIG. 5. Temperature response of AOGCMs with the highest ε value for the abrupt $4xCO_2$ and $1\%\ y^{-1}$ CO_2 experiments (grey dots) and corresponding fit for EBM-1 (dashed grey) and EBM-ε (thin black). Note that the EBM-1 and the EBM-ε solutions are superposed for the $1\%\ y^{-1}$ CO_2 and the beginning of the abrupt $4xCO_2$ experiments. The dotted lines denote the equilibrium temperature for EBM-1 (grey) and EBM-ε (black).

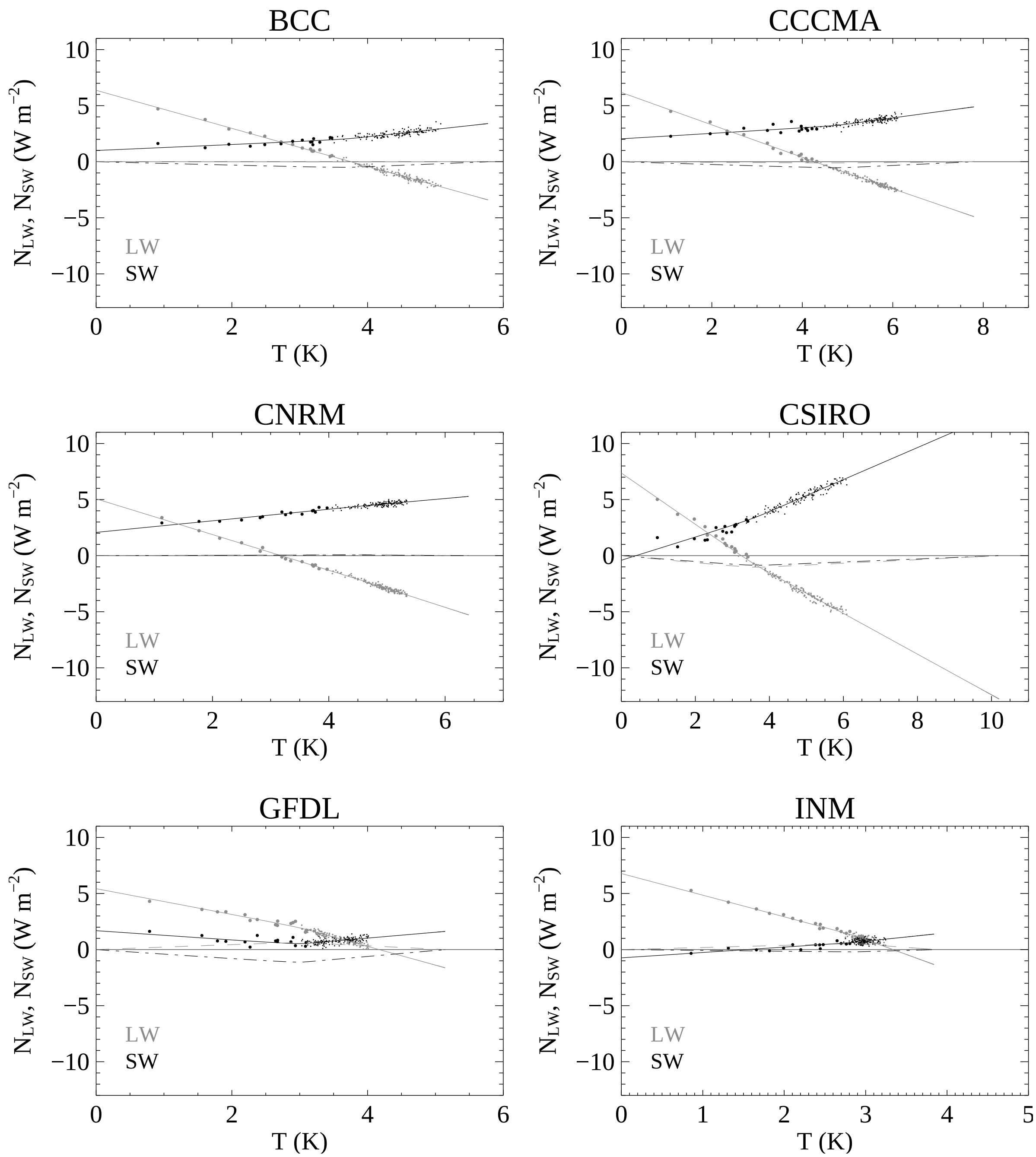

FIG. 6. Global mean net LW (grey) and SW (black) radiative flux at TOA as a function of global mean surface air temperature T for the abrupt 4xCO_2 experiments (black dots, large dots for the first 15 years), for the first 6 AOGCMs. The thick grey and black lines are the EBM-ε fits, respectively of the LW and the SW radiative flux. The grey dashed line and the black dot-dashed lines show, respectively, the LW and SW components of the $-(\varepsilon-1)H$ term. The thin black line shows $N = 0$. Note that the range of T can differ from one panel to another.

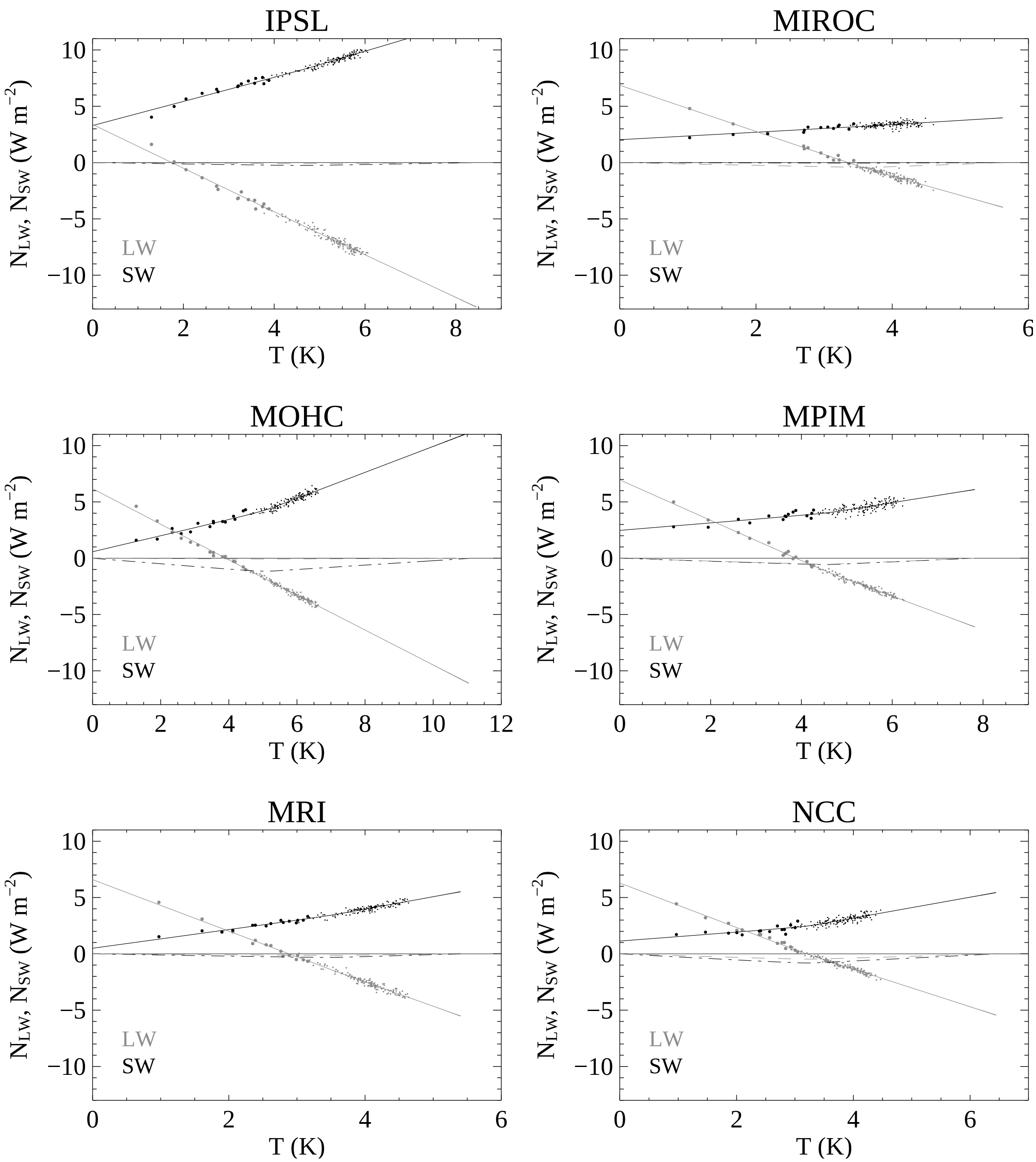

FIG. 7. Same as Fig. 6 for the 6 other AOGCMs.